BNL-223729-2022-JAAM

Ultra-fast non-equilibrium synthesis of cathode materials for Li-ion batteries

W. Zhu, E. Hu

To be published in "Advanced Materials"

November 2022

Chemistry Department

Brookhaven National Laboratory

U.S. Department of Energy

USDOE Office of Energy Efficiency and Renewable Energy (EERE), Vehicle Technologies Office (EE-3V)

DISCLAIMER

Ultra-fast non-equilibrium synthesis of cathode materials for Li-ion batteries

Wei Zhu,[1]† *Jingchao Zhang,*[1]† *Jiawei Luo,*[1]† *Cuihua Zeng,*[1]† *Hai Su,*[1] *Jinfeng Zhang,*[1] *Rui Liu,*[2] *Enyuan Hu,*[3] *Yuanshen Liu,*[1] *Wei-Di Liu,*[4] *Yanan Chen*[1,*] *Wenbin Hu*[1,*] *Yunhua Xu*[1*]

[1] School of Materials Science and Engineering, Key Laboratory of Advanced Ceramics and Machining Technology (Ministry of Education), and Tianjin Key Laboratory of Composite and Functional Materials, Tianjin University, Tianjin 300072, China.

[2] School of Materials Science and Engineering, Shandong University of Science and Technology, Qingdao, 266590, China.

[3] Chemistry Division, Brookhaven National Laboratory, Upton, NY 11973, USA.

[4] Australian Institute for Bioengineering and Nanotechnology, The University of Queensland, St Lucia, Brisbane, QLD 4069, Australia.

†These authors contributed equally to this work.

*Corresponding author. Email: yananchen@tju.edu.cn (Y. C.); wbhu@tju.edu.cn (W. H.); yunhua.xu@tju.edu.cn (Y. X.)

Keywords: Li-ion batteries, cathode materials, ultra-fast synthesis, high-temperature shock

Abstract

Synthesis of cathode materials plays an important role in determining the production efficiency, cost and performance of lithium-ion batteries. However, the conventional synthesis methods always experience a slow heating rate and involve a complicated multi-step reaction process and sluggish reaction dynamics, leading to high energy and long time consuming. Herein, we report a high-temperature shock (HTS) strategy for the ultra-fast synthesis of cathode materials in seconds. The HTS process experiences an ultra-high heating rate, leading to a non-equilibrium reaction and fast reaction kinetics and avoiding high energy and long time consuming. Mainstream cathode materials (such as $LiMn_2O_4$, $LiCoO_2$, $LiFePO_4$, and Li-rich layered oxide/NiO heterostructured material) are successfully synthesized with pure phases, oxygen vacancies, ultra-small particle sizes and good electrochemical performance. The HTS process not only provides an efficient synthesis approach for cathode materials but also can be extended beyond lithium-ion batteries.

1. Introduction

Li-ion batteries (LIBs) have been widely applied in electronics, electric vehicles, and large energy storage systems, and undergo a soaring demand for advanced LIBs with higher energy density and lower cost.[1] For practical applications of LIBs, cathode is the most important component to determine the energy density as well as cost. Various cathode materials have been developed, such as $LiCoO_2$, $LiMn_2O_4$, $LiFePO_4$, ternary layered materials $LiNi_xCo_yMn_zO_2$, and Li-rich layered materials $xLiMO_2 \cdot (1\text{-}x)Li_2MnO_3$ (M=Ni, Co, Mn).[2] Traditionally, these cathode materials are prepared by different methods, including solid-phase, sol-gel, co-precipitation, combustion, and spray drying methods.[3] All these methods require a long-time (usually several hours) heat treatment to produce fine crystalline structures, that takes place in a complicated reaction process with a low heating rate and sluggish reaction kinetics.[4] For example, the solid-state synthesis of $LiCoO_2$ involves multiple reaction

steps, including the melting/decomposing of salts, the diffusion of Li^+, and the rearrangement of crystal structures, taking a lot of time and energy.[4b] Therefore, there is an increasing need to develop new approaches to improve the synthesis efficiency and break the thermodynamic/kinetic limitations of the existing synthetic methods.

To address these challenges, rapid synthesis strategies were proposed, for instance, the emulsion process and microwave synthesis were used to synthesize cathode materials.[5] Emulsion is formed by dispersing a precursor solution into a immiscible liquid in the presence of surfactants, where there is a fast reaction speed due to the homogeneous dispersion of precursors.[5a] Microwave heating enables a rapid synthesis within several minutes through a direct absorption of microwave energy into the materials.[5b] Although these methods significantly reduce the synthesis time, the complicated multi-step reaction process is still necessary with limited reaction kinetics. Furthermore, the electrochemical performance of the resulting cathode materials is moderate and there is a large room for improvement.

In this work, we report an ultra-fast high-temperature shock (HTS) strategy to synthesize cathode materials through a non-equilibrium reaction, in which a high heating rate (~10^4 °C/min), high calcination temperature, high cooling rate (~10^3-10^4 °C/min), and fast reaction kinetics can be simultaneously achieved (Figure 1a).[6] Compared with the traditional synthesis methods that need a long-time heat treatment and multi-step reactions, the non-equilibrium feature of HTS enables a one-step reaction for the synthesis of cathode materials within a few seconds (Figure 1b). Furthermore, the non-equilibrium process tends to introduce oxygen vacancies and form small grains, that are beneficial to enhancing electrochemical performance. Using this method, typical cathode materials are synthesized, including $LiMn_2O_4$, $LiCoO_2$, $LiFePO_4$, and Li-rich layered oxide/NiO heterostructured material, and excellent electrochemical performances are demonstrated.

2. Results and discussion

To demonstrate the applicability of HTS, $LiMn_2O_4$, a typical cathode material used in LIBs, was synthesized. The precursor was prepared by a typical combustion method (as shown in the Experimental Section), and then calcined to form $LiMn_2O_4$ cathode material through the HTS process. A precalcination process was applied to remove organic components from the precursor at ~660°C for ~9 s. Then the resulting product was calcined at ~970°C for ~8 s to produce the final product of $LiMn_2O_4$ (Figure 1c). Although the synthesis is extremely fast with negligible ramping and cooling stages, a fine crystal structure was formed. For comparison, $LiMn_2O_4$ was also synthesized using a traditional long-time heat treatment method (Figure S1, Supporting Information).

The structure evolution during the HTS process was tracked by X-ray diffraction (XRD). Figure 1d shows the evolution of XRD patterns of the precursor and the intermediate product during the HTS processes. No diffraction peak was measured for the precursor, indicative of amorphous structure. While after an ultra-short time of precalcination for 4 s, a cubic $LiMn_2O_4$ phase was formed as revealed by the pronounced peaks in the XRD pattern, corresponding to *Fd-3m* space group. The formation of $LiMn_2O_4$ phase is accompanied by the generation of an impure phase of tetragonal Mn_3O_4, which may be attributed to the inadequate reaction due to a large amount of gas production from organic components. Even up to 10 s of precalcination, no obvious change was observed except a slight increase of the weight fraction of $LiMn_2O_4$ phase, as shown by the Rietveld refinement results of XRD data (Figure 1e). Note that no Li_2O was detected because it has an amorphous structure.[4b] During the calcination process, the peaks of Mn_3O_4 quickly disappeared after 2 s and a pure $LiMn_2O_4$ phase formed. These results indicate that the precursor can be directly converted into the final products of cathode materials in seconds without complicated multiple-step reactions that often take place in traditional methods.[4b,4c,7] Therefore, the HTS synthesis has actually a one-step formation process of cathode materials. The difference in the formation mechanism between the HTS and traditional synthesis methods lies in the different reaction kinetics. In the traditional methods, a low heating rate is applied, leading to slow reaction kinetics and multi-step reaction

processes. In contrast, the HTS method undergoes an ultra-high heating rate and a non-equilibrium reaction process, avoiding the low-temperature reaction. As a result, a fast reaction kinetics can be realized, promising a fast formation of the designed cathode materials through a one-step reaction. The structure evolution in the traditional heat-treatment method was monitored by XRD (Figure S2, Supporting Information). A two-step reaction with a slow reaction kinetics was clearly revealed, involving the decomposition of precursors and formation of Li_2O and Mn_3O_4 below 230 °C in the first step and a slow formation process of $LiMn_2O_4$ phase between 230-700 °C in the second step.

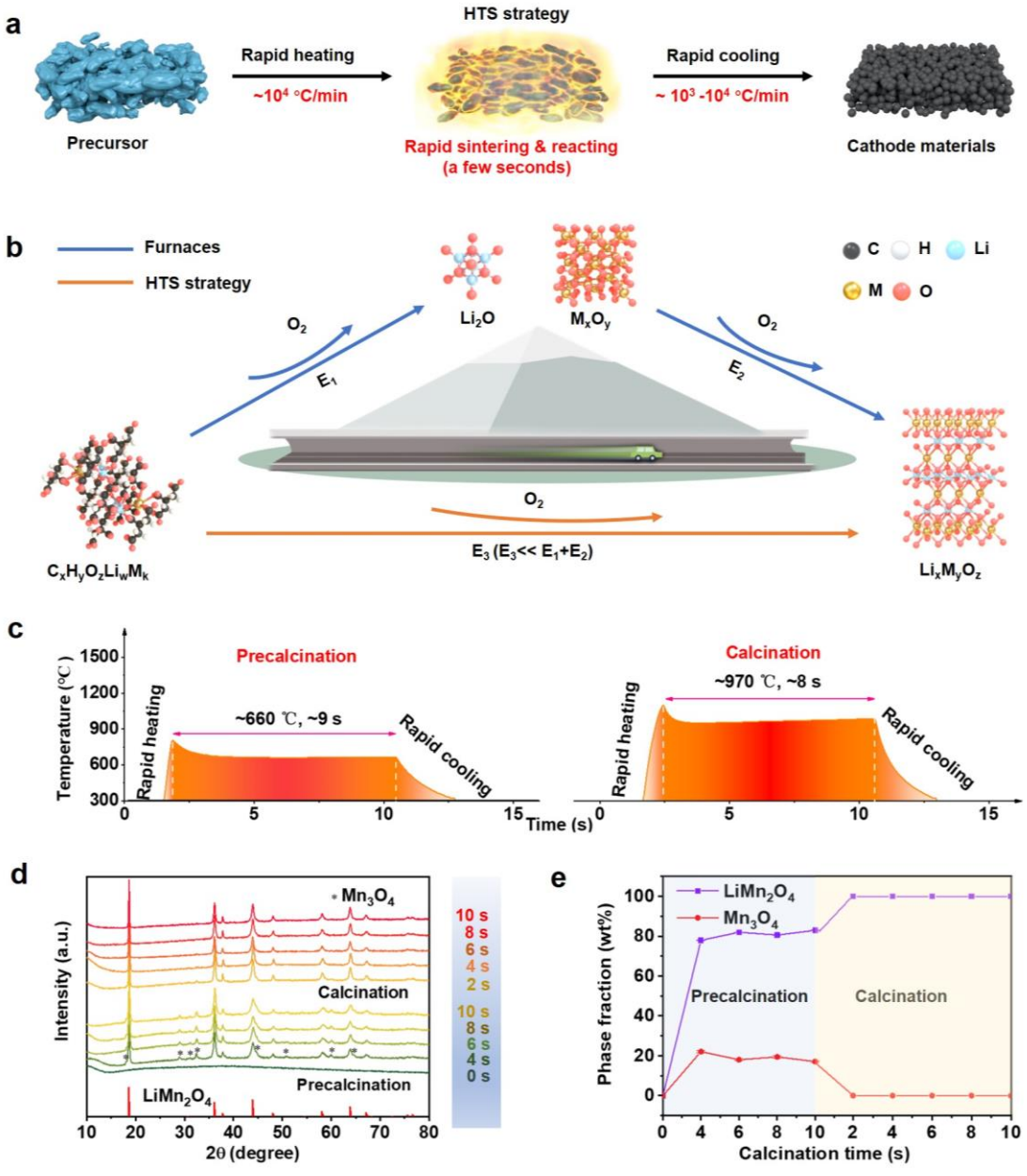

Figure 1. HTS synthesis of cathode materials. a) Schematic description of the HTS synthesis of cathode materials. b) Comparison of the reaction paths of the HTS and conventional synthesis methods. c) Temperature curve of the HTS process. d) XRD patterns evolution of the precursor of $LiMn_2O_4$ in the HTS process. e) A quantitative analysis of the weight fractions of different phases obtained from Rietveld refinement of the corresponding XRD data.

To have insights into the difference of the formation mechanisms of $LiMn_2O_4$ in the HTS and traditional synthesis processes, first-principles calculations were conducted. To simplify the computation, the precursor was assumed to be composed of $C_6H_6O_7Li_2$ and $C_6H_8O_8Mn$, and model structures of reactants and products involved in the structure transition processes were used to analyze Gibbs free energy (ΔG) at different temperatures (Figure S3, Supporting Information). In conventional synthesis, there exists a two-step reaction process. In Step 1, the precursor was converted into intermediate products, which include Li_2O and Mn_3O_4. In this process, ΔG is negative over the whole temperature range, indicating a spontaneous reaction (Figure 2a, c). While ΔG turns from positive to negative in Step 2 as temperature increases, in which Li_2O and Mn_3O_4 were transferred into $LiMn_2O_4$. Interestingly, a critical temperature (T_c) is displayed in Step 2, indicating that the reaction would irreversibly take place once the temperature reaches T_c (Figure 2b, c). Given a slow heating rate of 3 °C/min in the conventional synthesis, it will take a long time to reach T_c to form $LiMn_2O_4$. In contrast, in the HTS process, ΔG keeps negative, implying a spontaneous reaction (Figure 2d, e). Given the super-fast dynamics induced by the rapid heating in the HTS process, the precursor can be directly converted into $LiMn_2O_4$ in a very short time, and there is no intermediate reaction. This is consistent with the experimental results presented above.

The XRD pattern of the HTS-synthesized $LiMn_2O_4$ displays sharp diffraction peaks that can be well indexed to the cubic spinel phase, and no observable impurities were measured (Figure 3a). These results suggest a high crystallinity and phase purity, and the crystallographic parameters are listed in Table S1 (Supporting Information).

The phase purity is further confirmed by the inductively coupled plasma (ICP-OES) analysis (Table S2, Supporting Information).

The morphology of the HTS-synthesized $LiMn_2O_4$ was examined by scanning electron microscopy (SEM). A random shape was presented with particle sizes from 50 to 150 nm (Figure 3b), and a crystalline morphology can be clearly observed in the high-resolution SEM image (Figure 3c). The small particle sizes are preferred to achieve high electrochemical performance, such as high rate capability and good cycling stability.[3c] The formation of small particles should be attributed to the HTS process, in which the ultra-high heating rate induces a non-equilibrium reaction with a very fast reaction kinetics. The coarsening of the $LiMn_2O_4$ particles that often takes place in a low-temperature region and long-time heat treatment would not be able to occur in the HTS process.[5c]

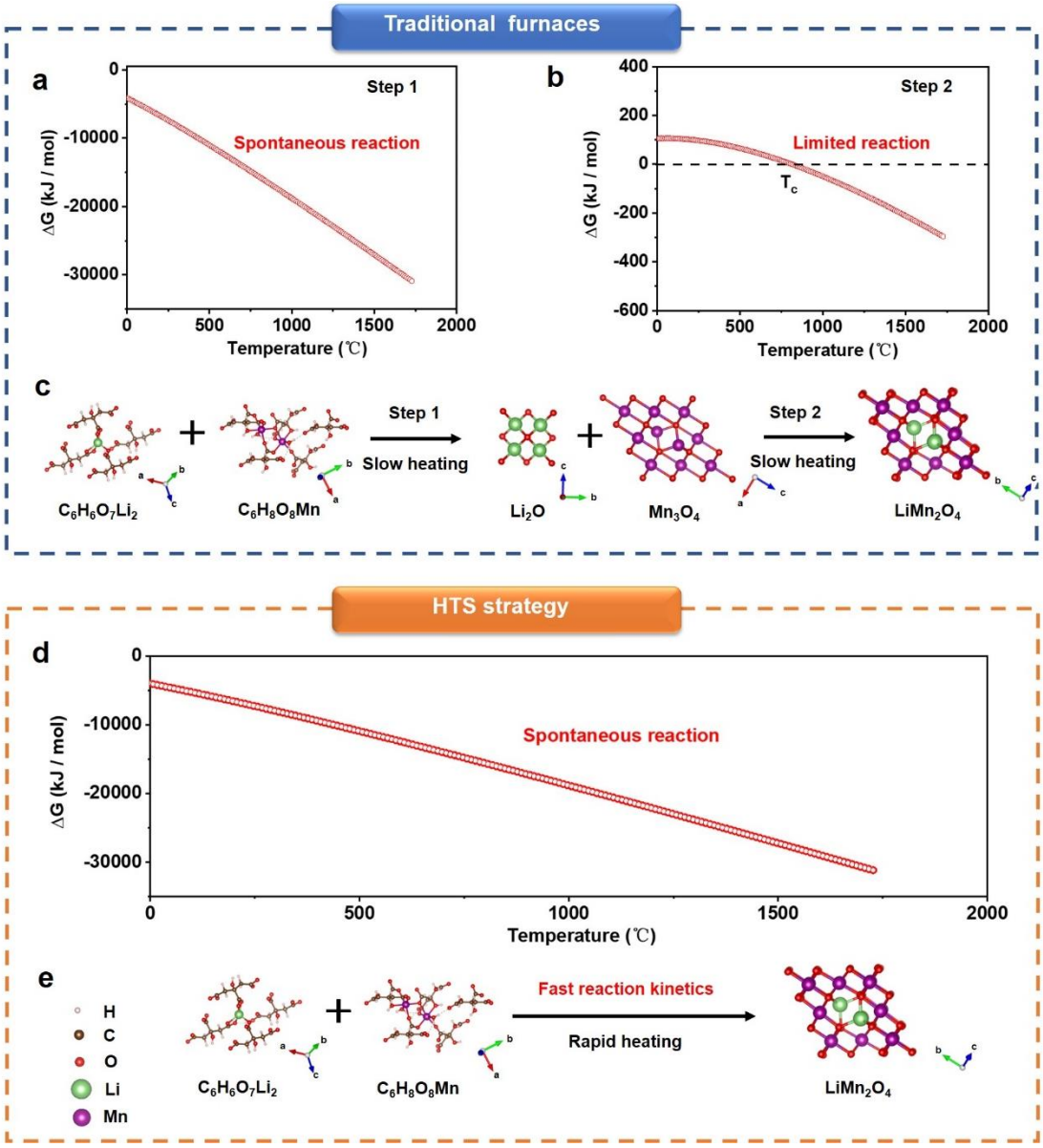

Figure 2. First-principles calculations for the formation processes of $LiMn_2O_4$ in HTS and traditional processes. ΔG of the reaction a) in Step 1 and b) Step 2 at different temperatures, and c) reaction pathways in the conventional process; d) ΔG of the reaction at different temperatures and e) reaction pathway in the HTS process.

The chemical properties of the HTS-synthesized $LiMn_2O_4$ were analyzed by X-ray photoelectron spectroscopy (XPS). The valence of Mn ion is calculated to be +3.35 based on the energy splitting between the Mn 3s peak and its satellite peak (Figure S4, Supporting Information), which is lower than those of $LiMn_2O_4$ cathode materials reported previously.[8] The decrease of chemical valence of Mn implies the

presence of oxygen vacancies that were produced by the high heating rate and short calcination time in the HTS process (Figure 3d). It has been reported that oxygen vacancies are beneficial to the diffusion of Li^+ and enhancement of electrochemical performance of cathode materials.[9]

The microstructure was investigated by scanning transmission electron microscopy (STEM) under a high-angle annular dark field (HAADF) mode. HAADF imaging is very sensitive to the crystalline structure and orientation of the tested materials. The diamond units consisted of Mn ions are clearly displayed in the STEM-HAADF image (Figure 3e), which is a typical characteristic of spinel structure with a space group of *Fd-3m* along the [011] zone axis. This is consistent with the XRD measurement results (Figure 3a). While Li and O ions are invisible in the HAADF image due to the mass-thickness contrast of ions.[10] The crystal lattice of $LiMn_2O_4$ was further illustrated by the corresponding atomic model of the HAADF image (Figure 3f). Oxygen anions are in a face-centered cubic arrangement, where Mn ions occupy one half of the octahedral sites and Li ions occupy one eighth of the tetrahedral sites. The energy dispersive x-ray spectroscopy (EDS) mapping images reveal a homogenous distribution of manganese and oxygen elements (Figure S5, Supporting Information), indicating that the spinel phase was uniformly formed in the HTS-synthesized $LiMn_2O_4$.

The electrochemical performance of $LiMn_2O_4$ was examined in a voltage window of 3.5-4.3 V. Figure 3g shows the galvanostatic charge-discharge profiles at a current rate of 0.1C. A typical curve shape is presented with two charge plateaus at 4.03/4.14 V and two discharge at 4.11/3.97 V, corresponding to a two-step extraction/insertion of Li^+ in the redox reaction of Mn^{3+}/Mn^{4+}. The two-step reaction was further revealed by the cyclic voltammetry (CV) curves at a scan rate of 0.1 mV s^{-1} (Figure S6, Supporting Information). $LiMn_2O_4$ delivers an initial discharge capacity of 116.9 mAh g^{-1} with a Coulombic efficiency of 88.2%. The galvanostatic cycling performance was tested at a current rate of 1C (Figure 3h, Figure S7, Supporting Information). A capacity retention of 82.5% is obtained after 100 cycles, which is similar to those reported $LiMn_2O_4$ cathode materials.[11] The capacity fading

can be attributed to two aspects. One is the dissolution of Mn^{2+} from by the disproportionation of Mn^{3+} (Figure S8, Supporting Information). The other is phase transition during cycling (Figure S9, 10, Supporting Information).[11a] Similar phenomenon has been reported in literature.[11a,12] The cycling performance of $LiMn_2O_4$ can be further improved through doping or coating.[11a,13] Furthermore, an excellent rate performance was obtained with a high capacity of 78.9 mAh g^{-1} at 5C, better than previously reported pure $LiMn_2O_4$ cathode materials (Figure 3i, Table S3, Supporting Information). This should be ascribed to the combination effects of three-dimension channels for Li^+ transportation, oxygen vacancies and small particles produced by the HTS process.[14] These results demonstrated that the HTS process is an effective approach for synthesizing high-performance cathode materials.

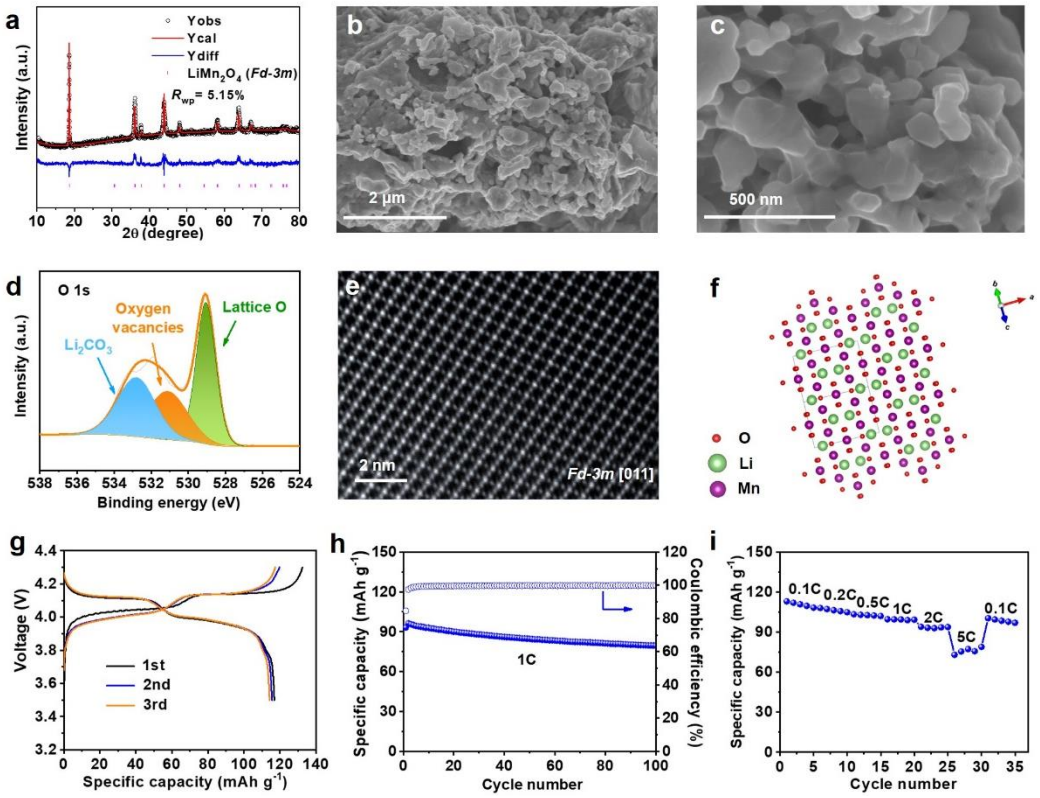

Figure 3. Structural characterization and electrochemical performance of the HTS-synthesized $LiMn_2O_4$. a) Refined XRD patterns, b, c) SEM image, d) O 1s XPS spectrum, e) STEM image, f) corresponding atomic mode, g) charge/discharge profiles at 0.1C within 3.5-4.3 V, h) cycling performance at 1C, and i) rate capability.

The universality of HTS in preparing cathode materials for LIBs was testified by

the successful synthesis of $LiCoO_2$ and $LiFePO_4$, and the synthesis details can be found in the Experimental Section, Figure S11-13, 22 (Supporting Information). Similar to $LiMn_2O_4$, a fine crystalline structure was formed with ultra-small particle sizes and abundant oxygen vacancies for $LiCoO_2$ (Figure 4a-c, Figure S14-17, Table S4-5, Supporting Information). As a result of the unique structures, a good cycling stability and outstanding rate capability were demonstrated by the HTS-synthesized $LiCoO_2$, including a reversible capacity of 139.5 mAh g^{-1} at 0.1C, a high capacity retention of 84.6% after 300 cycles at 1C, and a remarkable rate capability of 110.8 mAh g^{-1} at 5C (Figure 4d-f, Figure S18-21, and Table S6, Supporting Information). In addition to transition metal oxides, $LiFePO_4$ was also prepared by the HTS process with a good crystalline structure and good electrochemical performance (Figure S23-33, Table S7-8, Supporting Information).

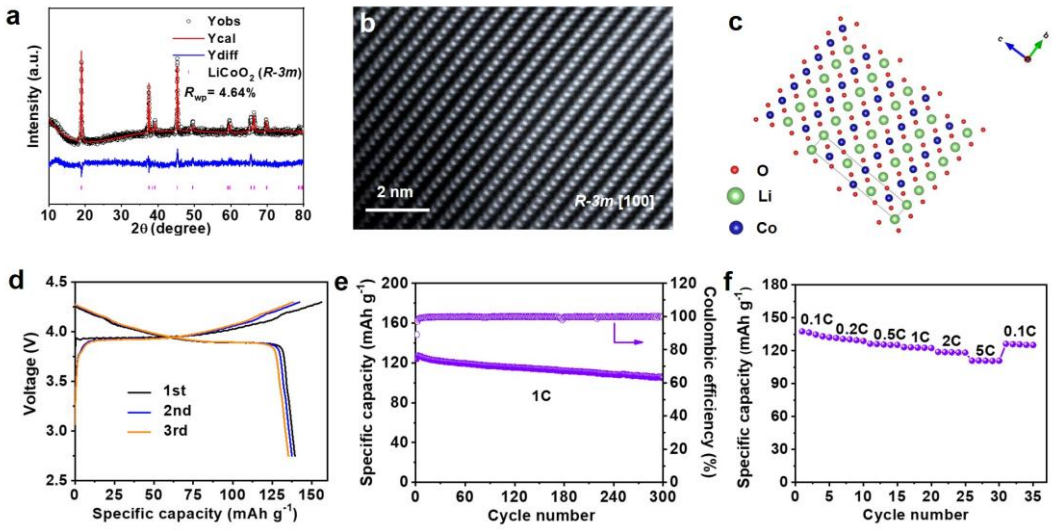

Figure 4. Structural characterization and electrochemical performance of the HTS-synthesized $LiCoO_2$. a) Refined XRD patterns, b) STEM image, c) corresponding atomic mode, d) charge/discharge profiles at 0.1C within 2.75-4.3 V, e) cycling performance at 1C, and f) the rate capability.

Compared with $LiMn_2O_4$ and $LiCoO_2$, Li-rich layered cathode materials have higher capacities and energy densities due to the involvement of both cations and anions in the electrochemical reactions.[15] However, the inferior cycling performance, induced by lattice oxygen release and phase transition from layered to spinel phase,

hinders their commercial application.[3d] It was reported that heterostructures by introducing other stable phases in the Li-rich layered material can enhance the structural stability and the electrochemical performance.[16] HTS provides a technology platform for fabricating heterostructured cathode materials because it has ultra-fast heating and quenching processes. In this work, Li-rich layered oxide/NiO heterostructured cathode material was synthesized using the HTS method, and the schematic synthesis process is schematically illustrated in Figure 5a (synthesis details can be found in the Experimental Section, Figure S34, Supporting Information). For the Li-rich layered oxide/NiO heterostructured cathode material, NiO-like phase can stabilize the structure of Li-rich layered cathode material owing to the potential pinning effects.[17] Similar to $LiMn_2O_4$ and $LiCoO_2$, the oxygen vacancies introduced by HTS can reduce oxygen loss at high voltage.[9a,17-18] Thus, a good cycling performance is expected for the Li-rich layered oxide/NiO heterostructured cathode material.

Similar to the aforementioned cathode materials, the ultra-small particle morphology and the oxygen vacancies were measured by SEM and XPS for the heterostructured cathode material (Figure S35-40, Supporting Information). The diffraction peaks of the heterostructured cathode material in the XRD pattern can be indexed to a layered phase of Li-rich layered oxide (space group: *R-3m* and *C2/m*) and NiO-like phase (space group: *Fm-3m*) (Figure 5b). The Rietveld refinement results reveal that the heterostructured cathode material consists of 94.7% layered phase and 5.3% NiO-like phase (Table S9, Supporting Information). The heterostructure was further verified by STEM. A mixed structure including the layered structure with space group *C2/m* in the [1-10] zone axis projection and the NiO salt structure with space group *Fm-3m* in the [01-1] zone axis projection can be clearly observed in Figure 5c. The two crystal structures and the corresponding atomic modes are presented in Figure 5d, e. Benefiting from the heterostructure with oxygen vacancies and small grain sizes, although the heterostructured cathode material exhibits a slightly lower discharge capacity than the reported Li-rich cathode materials in the literature due to the incorporation of electrochemically inert NiO, a good cycling

stability with no obvious capacity decay after 50 cycles and considerable rate capability are achieved (Figure 5f, g, Figure S41-44, Supporting Information).

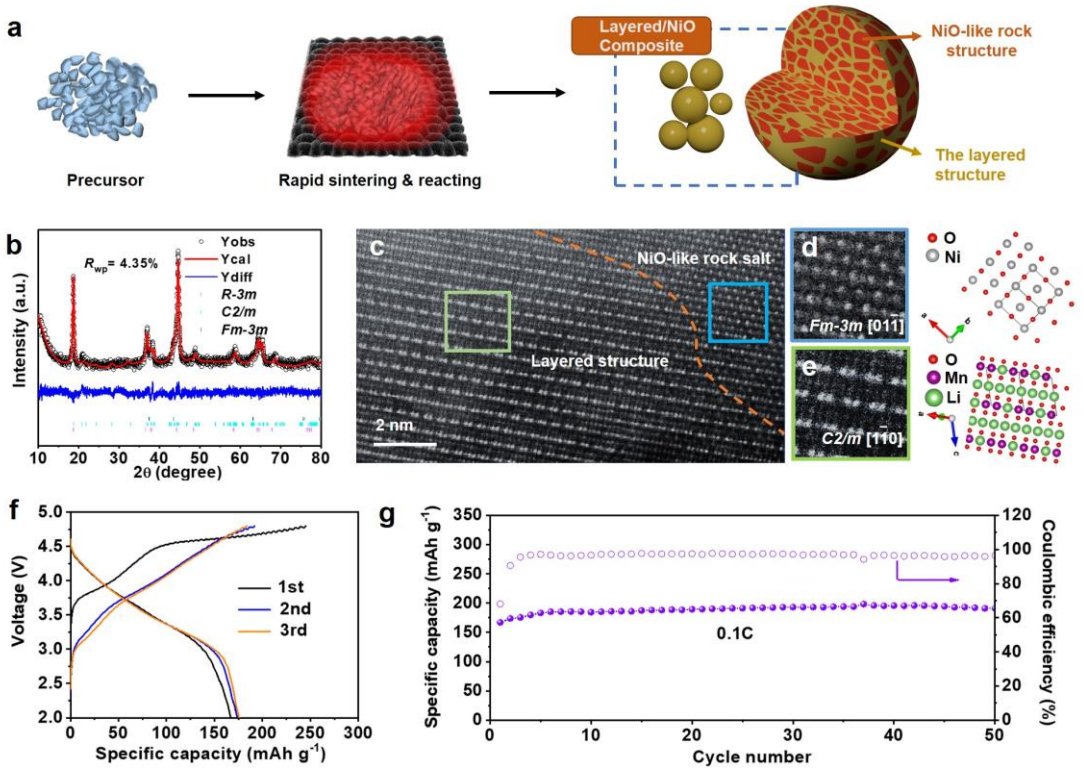

Figure 5. Synthesis, structural characterization and electrochemical performance of the HTS-synthesized Li-rich layered oxide/NiO heterostructured cathode material. a) Schematic illustration of the synthesis process, b) Refined XRD patterns, c) STEM image, and d) NiO phase and corresponding atomic mode, e) Li-rich layered oxide phase and corresponding atomic mode, f) charge/discharge profiles at 0.1C within 2-4.8 V, and g) cycling performance at 0.1C.

3. Conclusion and outlook

In summary, we have proposed a universal HTS strategy for synthesizing cathode materials in seconds. Different from traditional methods which usually experience a multi-step reaction process with limited chemical reaction kinetics and high energy and long time consuming, the HTS process provides an ultra-high heating rate, leading to a non-equilibrium state. This enables an ultra-fast one-step reaction, reducing energy consuming and saving time, and produces oxygen vacancies and forms ultra-small particles, promising high electrochemical performance. Typical cathode materials were synthesized, including $LiMn_2O_4$, $LiCoO_2$, $LiFePO_4$, and

Li-rich layered oxide/NiO heterostructured material, indicative of universality of the HTS synthesis method. Our findings open an efficient way for the synthesis of high-performance cathode materials.

In future work, there are several other potential applications in the cathode materials. First, excessive lithium replenishment is necessary to compensate the loss of lithium in conventional methods, which could lead to some difficulties in accurately controlling the chemical composition of the cathode material. However, owing to the extremely short synthesis time in the process of HTS, it is convenient for precisely controlling the composition of the cathode material. Second, defect engineering is an effective strategy for improving the electrochemical properties of cathode materials. Non-equilibrium property of HTS could synthesize cathode materials with point defect (oxygen vacancy), heterostructure, and dislocation which are in favor of promoting electrochemical performance. Third, the ability of HTS to rapidly synthesize a series of cathode materials can make us quickly screen and identify some new cathode materials based on artificial intelligence.

Experimental Section

Synthesis of the precursor of LMn_2O_4: The precursor of $LiMn_2O_4$ was synthesized using a combustion method. 0.1 mol $CH_3COOLi{\cdot}2H_2O$ (5 wt% excess, 99.9%, Meryer) and 0.2 mol $Mn(CH_3COO)_2{\cdot}4H_2O$ (99%, Heowns) were dissolved in anhydrous ethanol (80 ml) to form Solution A, and $C_6H_8O_7{\cdot}H_2O$ (0.2 mol, 99.5%, Aladdin) in anhydrous ethanol (80 ml) to form Solution B. Then Solutions A and B were simultaneously dropwise added to 200 ml anhydrous ethanol to generate a precipitate at 80 °C, and the precipitate was collected and dried at 100 °C.

Synthesis of the precursor of $LiCoO_2$: The precursor of $LiCoO_2$ was synthesized using a combustion method. 0.1 mol $CH_3COOLi{\cdot}2H_2O$ (5 wt% excess, 99.9%, Meryer) and 0.1 mol $Co(CH_3COO)_2{\cdot}6H_2O$ (98%, Heowns) were dissolved in deionized water (60 ml) to form Solution A, and $C_6H_8O_7{\cdot}H_2O$ (0.1 mol, 99.5%, Aladdin) in deionized water (60 ml) to form Solution B. Then Solutions A and B were simultaneously dropwise added to 150 ml deionized water to generate a precipitate at 80 °C, and the precipitate was collected and dried at 100 °C.

Synthesis of the precursor of $LiFePO_4$: The precursor of $LiFePO_4$ was synthesized using a spray drying method, which was purchased from Tianjin Koster Automotive Technology Company.

Synthesis of the precursor of Li-rich layered oxide/NiO heterostructured material: The precursor of Li-rich layered oxide/NiO was synthesized using a combustion method. 0.12 mol $CH_3COOLi{\cdot}2H_2O$ (5 wt% excess, 99.9%, Meryer), 0.02 mol $Ni(CH_3COO)_2{\cdot}4H_2O$ (99%, Heowns), and 0.06 mol $Mn(CH_3COO)_2{\cdot}4H_2O$ (99%, Heowns) were dissolved in anhydrous ethanol (50 ml) to form Solution A, and $C_6H_8O_7{\cdot}H_2O$ (0.1 mol, 99.5%, Aladdin) in anhydrous ethanol (50 ml) to form Solution B. Then Solutions A and B were simultaneously dropwise added to anhydrous ethanol (250 ml) at 80 °C to generate a precipitate, and the precipitate was collected and dried at 100 °C.

HTS process: A carbon cloth was used as a heater (5.0 cm ×2.5 cm , Taiwan Carbon energy Technology). It was powered by a DC power supply (MP50100D) in a current range of 0-100 A and a voltage range of 0-50 V. The temperature of the heater was tuned by adjusting the current and voltage and monitored by a laser infrared thermometer (Sanya Kechuang Future Technology). The HTS process was carried out in air for $LiMn_2O_4$, $LiCoO_2$, and Li-rich layered oxide/NiO and in argon for $LiFePO_4$. Besides, for the synthesis of $LiCoO_2$, an Al_2O_3 ceramic chip (20 mm×20 mm×0.65 mm, Foshan Hao Material New material technology) was employed as a sample holder, placed on the carbon cloth.

Material characterization: The crystal structure was analyzed by X-ray diffraction (XRD, D8 Advanced) with Cu Kα radiation (λ = 1.5406 Å, 40 kV and 40 mA).

Rietveld refinement was conducted using a GSAS code with EXPGUI interface.[19] Morphological investigation was conducted on a field emission scanning electron microscope (FSEM, s4800). Inductive coupled plasma technique (ICP-OES, Agilent 5110) was used to analyze the chemical composition of the materials. The chemical properties were analyzed by X-ray photoelectron spectroscopy (XPS, Axis Supra) and hard- X-Ray absorption spectroscopy (XAS, QAS (7-BM) beamline, Brookhaven National Laboratory). All XPS data were calibrated against the C1s peak at 284.6 eV. The valence state of Mn ions was calculated by the following equation: AOS=8.956-1.126ΔE (ΔE represents the splitting energy between the Mn 3s peak and its satellite peak). The X-ray absorption near edge structure (XANES) was processed using the Athena software package. Transmission electron microscopy (TEM, JEM-2100F) and aberration corrected TEM (JEM-ARM200F) equipped with energy-dispersive X-ray spectroscopy (EDS) were used to examine the microstructure and element distribution.

Electrochemical measurements: The cathode materials were mixed with Super P and polyvinylidene fluoride (PVDF) binder in a weight ratio of 8:1:1 and dispersed in N-methyl pyrrolidone (NMP) to make a slurry and cast onto carbon-coating aluminum foils. The electrodes were dried at 100 °C for 12 h in vacuum and the mass loading of the active material was about ~1.0 mg cm^{-2}. Coin cells (CR 2032) were assembled using lithium foils as counter electrodes, polypropylene separators (Celgard 2500, LLC Corp., USA), and electrolytes (For $LiMn_2O_4$ and $LiCoO_2$, the electrolyte formula was 0.8 M LiTFSI and 0.2 M LiDFBOP in FEC : EMC (3:7 by volume); For Li-rich layered oxide/NiO and $LiFePO_4$, a high-voltage electrolyte was purchased from DodoChem) in a glove box filled with highly pure argon gas (O_2 and H_2O levels < 0.1 ppm). Galvanostatic charge–discharge tests were carried out in a voltage range of 3.5-4.3 V for $LiMn_2O_4$, 2.75-4.3 V for $LiCoO_2$, 2.3-4.3 V for $LiFePO_4$, and 2.0-4.8 V for Li-rich layered oxide/NiO heterstructured cathode material. 1C corresponds to a current density of 148 mA g^{-1} for $LiMn_2O_4$, 140 mA g^{-1} for $LiCoO_2$, 170 mA g^{-1} for $LiFePO_4$, and 200 mA g^{-1} for Li-rich layered oxide/NiO heterstructured cathode material. Cyclic voltammetry (CV) measurements were performed on an electrochemistry workstation (CHI660E). Electrochemical impedance spectroscopy (EIS) data were recorded using a frequency response analyzer (1400, Solartron Analytical) coupled with an electrochemical interface (1470, Solartron Analytical) at an amplitude of 5 mV and a frequency range of 1 mHz to 1 MHz.

Theory calculations: First-principles calculations were carried out using the Vienna Ab initio Simulation Package (VASP).[20] The generalized gradient approximation (GGA) with Perdew Burke Ernzerhof (PBE) functional was used to process the exchange-correlation part. The projected augment plane wave (PAW) was used to describe the core-state of Li, Mn, H, C, and O elements. For $C_6H_6O_7Li_2$, $C_6H_8O_8Mn$, O_2, Mn_3O_4, Li_2O, H_2O, CO_2, and $LiMn_2O_4$ models, a cut-off energy of 500 eV was applied. The positions of all atoms and the cell parameters were relaxed until the

average force per atom decrease to 0.005 eV A^{-1}. The Brillouin zone integration was carried out by selecting a k-point mesh satisfied ka~30 A in different models. (2*2*2) supercells were employed for thermodynamic data and Phonon Spectrum calculations. All calculations are spin-polarized.

Acknowledgments: This work was financially supported by the National Natural Science Foundation of China (Grant No. 52171219, 91963113). This research used 7-BM beamline of the National Synchrotron Light Source II, U.S. DOE Office of Science User Facilities, operated for the DOE Office of Science by Brookhaven National Laboratory under contract no. DE-SC0012704.

Author contributions: Y. C., Y. X., and W. Z. conceived the concept and designed the experiments. W. Z., J. Z., J. L., and C. Z. carried out the synthesis and characterization. H. S. conducted electrochemical measurement and analysis. J. Z. and E. H. performed the characterization of TEM, STEM, and XAS. Y. L. performed the 3D illustrations. W. Z. wrote and Y. C., Y. X., W. H., W.-D. L. and R. L. revised the manuscript. All authors discussed the results and commented on the final manuscript.

Competing interests: The authors declare that they have no other competing interests.

Data and materials availability: All data are available in the manuscript or the supplementary materials.

References

[1] a) J. M. Tarascon, M. Armand, *Nature* **2001**, 414, 359; b) J. B. Goodenough, K. S. Park, *J. Am. Chem. Soc.* **2013**, 135, 1167; c) N. Nitta, F. X. Wu, J. T. Lee, G. Yushin, *Mater. Today* **2015**, 18, 252; d) S. S. Chen, D. Zhao, L. Chen, G. R. Liu, Y. Ding, Y. L. Cao, Z. X. Chen, *Small Struct.* **2021**, 2, 2100082; e) J. Kim, H. Lee, H. Cha, M. Yoon, M. Park, J. Cho, *Adv. Energy Mater.* **2018**, 8, 1702028; f) E. M. Hitz, H. Xie, Y. Lin, J. W. Connell, G. W. Rubloff, C. F. Lin, L. B. Hu, *Small Struct.* **2021**, 2, 2100014; g) J. C. Zhang, Z. D. Liu, C. H. Zeng, J. W. Luo, Y. D. Deng, X. Y. Cui, Y. N. Chen, *Rare Met.* **2022**, 41, 3946.

[2] a) A. Manthiram, *Nat. Commun.* **2020**, 11, 1550; b) J. L. Shi, D. D. Xiao, M. Y. Ge, X. Q. Yu, Y. Chu, X. J. Huang, X. D. Zhang, Y. X. Yin, X. Q. Yang, Y. G. Guo, L. Gu, L. J. Wan, *Adv. Mater.* **2018**, 30, 1705575; c) M. Li, J. Lu, Z. W. Chen, K. Amine, *Adv. Mater.* **2018**, 30, 1800561.

[3] a) A. H. Marincas, F. Goga, S. A. Dorneanu, P. Ilea, *J. Solid State Electrochem.* **2020**, 24, 473; b) W. J. Zhang, *J. Power Sources* **2011**, 196, 2962; c) E. Antolini, *Solid State Ionics* **2004**, 170, 159; d) J. M. Zheng, S. J. Myeong, W. R. Cho, P. F. Yan, J. Xiao, C. M. Wang, J. Cho, J. G. Zhang, *Adv. Energy Mater.* **2017**, 7, 1601284.

[4] a) D. G. Tong, Q. Y. Lai, J. Z. Lu, N. N. Wei, X. Y. Ji, *Chin. Sci. Bull.* **2005**, 50, 1087; b) S. A. Wicker, E. H. Walker, *Inorg. Chem.* **2013**, 52, 1772; c) S. N. Wang, W. B. Hua, A. Missyul, M. S. D. Darma, A. Tayal, S. Indris, H. Ehrenberg, L. J. Liu, M. Knapp, *Adv. Funct. Mater.* **2021**, 31, 2009949.

[5] a) C. H. Lu, P. Y. Yeh, *J. Mater. Chem.* **2000**, 10, 599; b) M. Nakayama, K. Watanabe, H. Ikuta, Y. Uchimoto, M. Wakihara, *Solid State Ionics* **2003**, 164, 35; c) H. Yan, X. Huang, L. Zhonghua, H. Huang, R. Xue, L. Chen, *J. Power Sources* **1997**, 68, 530; d) S. Beninati, L. Damen, M. Mastragostino, *J. Power Sources* **2008**, 180, 875.

[6] a) Y. N. Chen, G. C. Egan, J. Y. Wan, S. Z. Zhu, R. J. Jacob, W. B. Zhou, J. Q. Dai, Y. B. Wang, V. A. Danner, Y. G. Yao, K. Fu, Y. B. Wang, W. Z. Bao, T. Li, M. R. Zachariah, L. B. Hu, *Nat. Commun.* **2016**, 7, 12332; b) S. M. Dou, J. Xu, X. Y. Cui, W. D. Liu, Z. C. Zhang, Y. D. Deng, W. B. Hu, Y. N. Chen, *Adv. Energy Mater.* **2020**, 10, 2001331; c) Z. D. Liu, C. P. Duan, S. M. Dou, Q. Y. Yuan, J. Xu, W. D. Liu, Y. N. Chen, *Small.* **2022**, 18, 8; d) C. Liu, W. Zhou, J. Zhang, Z. Chen, S. Liu, Y. Zhang, J. Yang, L. Xu, W. Hu, Y. Chen, Y. Deng, *Adv. Energy Mater.* **2020**, 10, 2001397; e) S. Liu, Y. Shen, Y. Zhang, B. Cui, S. Xi, J. Zhang, L. Xu, S. Zhu, Y. Chen, Y. Deng, W. Hu, *Adv. Mater.* **2022**, 34, 2106973; f) C. Liu, Y. Shen, J. F. Zhang, G. Li, X. R. Zheng, X. P. Han, L. Y. Xu, S. Z. Zhu, Y. A. Chen, Y. D. Deng, W. B. Hu, *Adv. Energy Mater.* **2022**, 12, 9; g) S. L. Liu, Z. Hu, Y. Z. Wu, J. F. Zhang, Y. Zhang, B. H. Cui, C. Liu, S. Hu, N. Q. Zhao, X. P. Han, A. Y. Cao, Y. N. Chen, Y. D. Deng, W. B. Hu, *Adv. Mater.* **2020**, 32, 8.

[7] M. J. Zhang, Y. D. Duan, C. Yin, M. F. Li, H. Zhong, E. Dooryhee, K. Xu, F. Pan, F. Wang, J. M. Bai, *Sci. Adv.* **2020**, 6, eabd9472.

[8] M. Jeong, M. J. Lee, J. Cho, S. Lee, *Adv. Energy Mater.* **2015**, 5, 1500440.
[9] a) B. Qiu, M. H. Zhang, L. J. Wu, J. Wang, Y. G. Xia, D. N. Qian, H. D. Liu, S. Hy, Y. Chen, K. An, Y. M. Zhu, Z. P. Liu, Y. S. Meng, *Nat. Commun.* **2016**, 7, 12108; b) W. Q. Xu, Y. H. Zheng, L. N. Lin, W. B. Lei, Z. G. Wang, H. L. Song, Y. Cheng, R. J. Qi, H. Peng, H. C. Lin, Z. Z. Yang, R. Huang, *J. Alloys Compd.* **2021**, 870, 159387.
[10] C. D. Amos, M. A. Roldan, M. Varela, J. B. Goodenough, P. J. Ferreira, *Nano letters* **2016**, 16, 2899.
[11] a) T. C. Liu, A. Dai, J. Lu, Y. F. Yuan, Y. G. Xiao, L. Yu, M. Li, J. Gim, L. Ma, J. J. Liu, C. Zhan, L. X. Li, J. X. Zheng, Y. Ren, T. P. Wu, R. Shahbazian-Yassar, J. G. Wen, F. Pan, K. Amine, *Nat. Commun.* **2019**, 10, 4721; b) B. J. Kwon, F. Dogan, J. R. Jokisaari, B. Key, C. Kim, Y. S. Liu, J. H. Guo, R. F. Klie, J. Cabana, *ACS Appl. Mater. Interfaces* **2019**, 11, 3823; c) S. Zhao, Y. Bai, L. H. Ding, B. Wang, W. F. Zhang, *Solid State Ionics* **2013**, 247, 22.
[12] J. C. Zhang, J. Wen, W. D. Liu, X. Y. Cui, Y. A. Chen, *Sci. China Mater.* **2022**, 65, 2613.
[13] a) M. J. Lee, S. Lee, P. Oh, Y. Kim, J. Cho, *Nano Letters* **2014**, 14, 993; b) A. Ahuja, A. Kumar, A. Sengupta, M. Gautam, H. Lohani, P. Kumari, S. Mitra, *Energy Storage Mater.* **2022**, 52, 169.
[14] Y. M. Huang, Y. H. Dong, S. Li, J. Lee, C. Wang, Z. Zhu, W. J. Xue, Y. Li, J. Li, *Adv. Energy Mater.* **2021**, 11, 869113.
[15] a) J. Zhang, Q. C. Wang, S. F. Li, Z. S. Jiang, S. Tan, X. L. Wang, K. Zhang, Q. X. Yuan, S. J. Lee, C. J. Titus, K. D. Irwin, D. Nordlund, J. S. Lee, P. Pianetta, X. Q. Yu, X. H. Xiao, X. Q. Yang, E. Y. Hu, Y. J. Liu, *Nat. Commun.* **2020**, 11, 6342; b) Y. Chen, Y. Liu, J. Zhang, H. Zhu, Y. Ren, W. Wang, Q. Zhang, Y. Zhang, Q. Yuan, G.-X. Chen, L. C. Gallington, K. Li, X. Liu, J. Wu, Q. Liu, Y. Chen, *Energy Storage Mater.* **2022**, 51, 756; c) Y. Liu, Y. Chen, J. Wang, W. Wang, Z. Ding, L. Li, Y. Zhang, Y. Deng, J. Wu, Y. Chen, *Nano Research* **2021**, 15, 3178.
[16] a) A. Bhaskar, S. Krueger, V. Siozios, J. Li, S. Nowak, M. Winter, *Adv. Energy Mater.* **2015**, 5, 1401156; b) Y. Pei, C. Y. Xu, Y. C. Xiao, Q. Chen, B. Huang, B. Li, S. Li, L. Zhen, G. Z. Cao, *Adv. Funct. Mater.* **2017**, 27, 1604349; c) M. Xu, L. F. Fei, W. Lu, Z. Y. Chen, T. Li, Y. Liu, G. Y. Gao, Y. Q. Lai, Z. A. Zhang, P. Wang, H. T. Huang, *Nano Energy* **2017**, 35, 271; d) H. C. Guo, Z. Wei, K. Jia, B. Qiu, C. Yin, F. Q. Meng, Q. H. Zhang, L. Gu, S. J. Han, Y. Liu, H. Zhao, W. Jiang, H. F. Cui, Y. G. Xia, Z. P. Liu, *Energy Storage Mater.* **2019**, 16, 220.
[17] C. X. Zhang, Y. Z. Feng, B. Wei, C. P. Liang, L. J. Zhou, D. G. Ivey, P. Wang, W. F. Wei, *Nano Energy* **2020**, 75, 104995.
[18] Q. Li, D. Ning, D. Wong, K. An, Y. Tang, D. Zhou, G. Schuck, Z. Chen, N. Zhang, X. Liu, *Nat. Commun.* **2022**, 13, 1123.
[19] B. H. Toby, *J. Appl. Crystallogr.* **2001**, 34, 210.
[20] G. K. A, J. F. b, *Comput. Mater. Sci.* **1996**, 6, 15.

The table of contents entry

An ultra-fast high-temperature shock strategy is proposed to synthesize cathode materials in seconds for lithium-ion batteries, avoiding high-energy and long-time consuming. It provides an ultra-high heating rate, leading to a non-equilibrium reaction and fast reaction kinetics. Mainstream cathode materials are successfully synthesized with pure phases, oxygen vacancies, ultra-small particle sizes, and good electrochemical performance, indicative of a universal and efficient synthesis approach.

Wei Zhu, Jingchao Zhang, Jiawei Luo, Cuihua Zeng, Hai Su, Jinfeng Zhang, Rui Liu, Enyuan Hu, Yuanshen Liu, Wei-Di Liu, Yanan Chen, Wenbin Hu,* Yunhua Xu**

Ultra-fast non-equilibrium synthesis of cathode materials for Li-ion batteries